International Journal of Statistics and Applied Mathematics

ISSN: 2456-1452
NAAS Rating (2026): 4.49
Maths 2026; 11(1): 08-18

https://www.mathsjournal.com
Received: 04-10-2025
Accepted: 08-11-2025

V Munaiah
Lecturer, Department of Statistics, SVA Government College, Srikalahasti, Andhra Pradesh, India

T Gangaram
Lecturer, Department of Statistics, SVA Government College, Srikalahasti, Andhra Pradesh, India

G Satyanarayanareddy
Lecturer, Department of Statistics, Government College for Men (A), Kadapa, Andhra Pradesh, India

J Kishore Kumar
Associate Professor, Department of Statistics, Maharani Science College for Women, Bangalore, Karnataka, India

Corresponding Author:
V Munaiah
Lecturer, Department of Statistics, SVA Government College, Srikalahasti, Andhra Pradesh, India

Modeling couple stress effects in Oldroyd-b fluid flow over a wedge: A multiple linear regression and Bayesian neural network approach

V Munaiah, T Gangaram, G Satyanarayanareddy and J Kishore Kumar

DOI: https://www.doi.org/10.22271/maths.2026.v11.i1a.2234

Abstract
This study investigates the steady, magnetohydrodynamic flow and heat transfer of an Oldroyd-B fluid over a wedge, incorporating the effects of thermal radiation, Joule heating, and couple stresses. The governing partial differential equations are reduced to a system of coupled ordinary differential equations through a set of suitable similarity transformations. The resulting nonlinear boundary value problem is solved numerically using the bvp4c solver in MATLAB, which employs a collocation scheme to achieve high-accuracy solutions. From the numerical data, predictive models for the skin friction coefficient and Nusselt number are developed via multiple linear regression, establishing quantitative relationships with key governing parameters. To ensure robustness and quantify predictive uncertainty, the regression outcomes are validated using a Bayesian neural network framework. The analysis demonstrates that increasing the couple stress parameter and magnetic field decelerates the flow, while the thermal radiation parameter and Eckert number significantly elevate the fluid temperature and entropy generation. The findings of this work have direct implications for optimizing thermal management systems, polymer processing flows, and the design of wedge-shaped components in aerospace and energy applications where viscoelastic fluid behavior and entropy minimization are critical.

Keywords: MHD, bvp4c, viscous dissipation, entropy generation, thermal radiation

Introduction
The study of non-Newtonian fluid flow over a wedge holds significant practical value across multiple engineering and industrial domains. This configuration is commonly encountered in aerodynamic designs, polymer processing, and thermal management systems, where fluid behavior deviates from Newtonian assumptions due to shear-thinning, viscoelastic, or time-dependent properties. Analyzing such flows helps optimize the performance of wedge-shaped components in heat exchangers, aircraft wings, and extrusion dies. Additionally, in biomedical and chemical engineering, understanding how these fluids interact with wedgelike geometries aids in improving drug delivery systems, filtration processes, and the design of microfluidic devices, ensuring enhanced efficiency, stability, and control in real-world applications. The study by Dawar *et al.* [1] examines convective flow of a Williamson nanofluid over cone and wedge geometries under non-isothermal and non-isosolutal conditions, applying a revised Buongiorno model with HAM for solution. Velocity enhancement was more significant for the cone compared to the wedge, while reductions in thermal and concentration profiles were greater for Williamson nanofluids than Newtonian ones. Shahzad *et al.* [2] numerically investigated the unsteady flow of a tangent hyperbolic nanofluid past a wedge with suction/injection, employing similarity transformations and solving the resulting ODEs with MATLAB's bvp4c and MAPLE's d-solve commands. The study determined that increasing the Weissenberg number reduces velocity but elevates temperature and concentration profiles. Kudenatti *et al.* [3] numerically analyzed the magnetohydrodynamic boundary layer flow of a non-Newtonian power-law fluid over a moving wedge using Chebyshev collocation and shooting methods, and conducted a linear stability analysis on the dual solutions obtained. The study revealed that dual solutions exist for certain parameter ranges, with the first solution

being stable and physically feasible while the second is unstable. Dharmaiah *et al*. [4] numerically investigated the magnetohydrodynamic free convection flow of a Casson nanofluid over a melting wedge, incorporating Joule heating, thermodiffusion, and chemical reaction effects using similarity transformations and MATLAB's bvp4c solver. The melting process was found to increase the thicknesses of momentum, thermal, and solutal boundary layers while reducing skin friction and heat and mass transfer rates. Zulqarnain *et al*. [5] conducted a numerical investigation of Darcy-Forchheimer Maxwell tri-hybrid nanofluid flow across a Riga wedge, considering nonlinear thermal radiation, mixed convection, and boundary slip effects using MATLAB's bvp4c solver. The study showed that increasing the wedge angle, Grashof numbers, and Maxwell fluid parameter enhances flow velocity, while higher nanoparticle volume fractions and porosity reduce it. Bagh Ali *et al*. [6] numerically investigated the effects of bioconvection and thermal radiation on magnetohydrodynamic nanofluid flow across a porous, stretching wedge using similarity transformations and the shooting technique with Range-Kutta integration in MATLAB. Later, various researchers [7-10] discussed different non-Newtonian fluid flows over wedge in the presence of several parameters, including magnetic field parameter.

Entropy generation analysis in non-Newtonian fluid flow is crucial for optimizing thermal and fluid systems, as it quantifies irreversibility due to heat transfer, fluid friction, and mass diffusion. By minimizing entropy production, engineers can design more efficient processes in industries such as polymer processing, enhanced oil recovery, microfluidics, and cooling systems, where non-Newtonian behavior-like shear-thinning or viscoelasticity-significantly impacts energy losses. This approach helps improve energy utilization, reduce operational costs, and enhance the sustainability of thermal management and chemical engineering applications. Acharya *et al*. [11] employed the Spectral Quasi-Linearization Method (SQLM) to analyze entropy generation in mixed convective, radiative couple-stress fluid flow over a permeable stretching cylinder under a magnetic field. The study revealed that entropy generation rises with increasing magnetic parameter, Reynolds number, and radiation, but declines with greater temperature difference. Ullah *et al*. [12] analyzed unsteady free convection of power-law fluid with thermal radiation and magnetic field, employing the finite difference method (FDM) to solve dimensionless governing equations for entropy generation and heat transfer. The study revealed that the entropy generation escalates with greater Eckert number and Grashof number. Berrehal *et al*. [13] numerically analyzed the steady, incompressible laminar flow of an aqueous Fe_3O_4-GO hybrid nanofluid over a convectively heated moving wedge, incorporating thermal radiation effects. Their study employed a novel mass-based modeling approach within the single-phase Tiwari-Das framework, combined for the first time with entropy generation analysis, and solved the governing equations using the Runge-Kutta-Fehlberg method with a shooting technique. The results indicated that increasing the wedge angle and the mass of graphene oxide nanoparticles enhanced entropy generation while reducing the Bejan number. Reedy *et al*. [14] numerically examined the entropy generation in a fully developed heat transport of a Carreau fluid flowing through a porous vertical microchannel. The study considered the effects of thermal radiation, viscous heating, a Darcy-Forchheimer porous model, and convective boundary conditions, solving the governing equations using the bvp4c method in MATLAB. The analysis revealed that increasing the Weissenberg number reduced entropy generation near the channel walls while enhancing the Bejan number, which peaked at the channel's centre. Later, various researchers [15-20] examined the entropy generation optimization in several fluid flows across different geometries.

Based on the comprehensive review of the literature, a research gap is identified concerning the integrated analysis of entropy generation, couple stress effects, and advanced data-driven modeling in the context of Oldroyd-B fluid flow over a wedge. While prior studies have explored various non-Newtonian models over similar geometries, there is a lack of work that systematically combines a detailed thermodynamic irreversibility analysis with modern predictive computational techniques. To address this gap, the present study formulates the flow problem incorporating thermal radiation, Joule heating, and couple stresses. Its principal novelty lies in the development and validation of robust, data-driven predictive models for key engineering outputs. Specifically, this research advances the field by deriving explicit multiple linear regression correlations for the skin friction coefficient and Nusselt number directly from high-fidelity numerical simulations. The reliability and uncertainty of these empirical models are rigorously assessed using a Bayesian neural network framework, offering a probabilistic validation method rarely applied in this domain. By bridging traditional fluid mechanics analysis with statistical learning and machine learning tools, this work provides a dual-methodology framework that enhances predictive capability and design insight. The results hold significant potential for improving the efficiency of industrial applications such as the thermal management of polymer processing equipment, the design of aerodynamic surfaces in contact with viscoelastic fluids, and the optimization of energy systems where minimizing entropy generation is paramount.

Formulation of the study

This study investigates the effect of several parameters, including couple stress and Joule heating, on the steady-state movement of an Oldroyd-B fluid across an angled wedge. In this investigation, we presuppose the following:

- Thermal radiation follows the Rosseland approximation.
- The flow is influenced by an externally applied vertical magnetic field of strength B, as illustrated in Fig. 1.
- Induced magnetic field effects are disregarded since the magnetic Reynolds number is small.

The subsequent circumstances and equations are requisite for this study, predicated on the aforementioned assumptions:

$$\frac{\partial u}{\partial x}+\frac{\partial v}{\partial y}=0 \tag{1}$$

$$u\frac{\partial u}{\partial x}+v\frac{\partial u}{\partial y}=\upsilon\frac{\partial^2 u}{\partial y^2}-\lambda_1\left(u^2\frac{\partial^2 u}{\partial x^2}+2uv\frac{\partial^2 u}{\partial x\partial y}+v^2\frac{\partial^2 u}{\partial y^2}\right)+g\beta_T\left(T-T_\infty\right)\sin\frac{\alpha}{2}$$
$$+\upsilon\lambda_2\left(u\frac{\partial^3 u}{\partial x\partial y^2}+v\frac{\partial^3 u}{\partial y^3}-\frac{\partial u}{\partial x}\frac{\partial^2 u}{\partial y^2}-\frac{\partial u}{\partial y}\frac{\partial^2 v}{\partial y^2}\right)-\frac{\sigma uB^2}{\rho}-\frac{\gamma_1}{\rho}\left(\frac{\partial^4 u}{\partial y^4}\right) \quad (2)$$

$$u\frac{\partial T}{\partial x}+v\frac{\partial T}{\partial y}=\frac{k}{\rho C_p}\frac{\partial^2 T}{\partial y^2}+\frac{1}{\rho C_p}\frac{16}{3}\frac{\sigma^* T_\infty^3}{k^*}\frac{\partial^2 T}{\partial y^2}+\frac{\mu}{\rho C_p}\left(\frac{\partial u}{\partial y}\right)^2+\frac{\sigma B^2}{\rho C_p}u^2 \quad (3)$$

$$\left.\begin{aligned}&u=u_w=ax^n, v=0, \frac{\partial^2 u}{\partial y^2}=0, k\frac{\partial T}{\partial y}=h_f\left(T-T_w\right)\ \text{at}\ y=0,\\&u\to 0, \frac{\partial u}{\partial y}\to 0, T\to T_\infty\ \text{as}\ y\to\infty.\end{aligned}\right\} \quad (4)$$

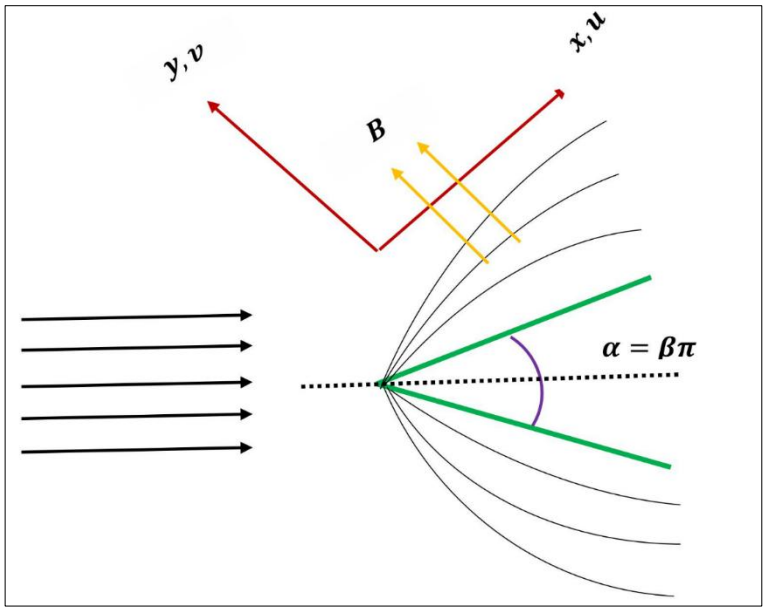

Fig 1: Graphical depiction of the current research

Bilal *et al*. [21] proposed the subsequent similarity transforms to translate governing equations:

$$\left.\begin{aligned}&u=u_w f'(\eta), v=-\sqrt{\frac{n+1}{2}}\sqrt{\frac{\upsilon u_w}{x}}\left[f(\eta)+\frac{n-1}{n+1}\eta f'(\eta)\right],\\&T=T_\infty+\left(T_w-T_\infty\right)\theta(\eta), T_w-T_\infty=T_0Ax^m, \eta=y\sqrt{\frac{n+1}{2}}\sqrt{\frac{u_w}{\upsilon x}}.\end{aligned}\right\} \quad (5)$$

The terms shown in (5) easily satisfy Equation (1). The following outcome results from the effective modification of equations (2-3) and conditions in (4) by the use of integration of (5):

$$\frac{n+1}{2}f'''-nf'^2+\frac{n+1}{2}ff''-\Lambda_1\left(\begin{aligned}&n(n-1)f'^3+\frac{(n-1)(2n^2-5n+1)}{4}\eta f'^2 f''\\&-\frac{(n-1)(3n-1)}{2}ff'f''+\left(\frac{n+1}{2}\right)^2 f^2 f'''\end{aligned}\right)$$
$$+\Lambda_2\left(\frac{(n+1)(n-1)}{2}f'f'''-\left(\frac{n+1}{2}\right)^2 ff^{iv}+\frac{(n+1)(3n-1)}{4}f''^2\right) \quad (6)$$
$$+\lambda\theta\sin\frac{\alpha}{2}-Mf'-\left(\frac{n+1}{2}\right)^2 Csf^v=0$$

$$\frac{n+1}{2}\frac{1}{\Pr}\theta''+\frac{n+1}{2}\frac{R}{\Pr}\theta''+\frac{n+1}{2}f\theta'-mf'\theta+\frac{n+1}{2}Ecf''^{2}+MEcf'^{2}=0 \tag{7}$$

$$\left.\begin{array}{l}\text{at } \eta=0: f(\eta)=0, f'(\eta)=1, f'''(\eta)=0, \theta'(\eta)=-Bi\left(1-\theta(\eta)\right),\\ \text{as } \eta\to 0: f'(\eta)\to 0, f''(\eta)\to 0, \theta(\eta)\to 0.\end{array}\right\} \tag{8}$$

where

$$\left.\begin{array}{l}Cs=\frac{\gamma_1 a}{\rho\upsilon^{2}}, \gamma_1=\gamma_0 x^{n-1}, M=\frac{\sigma B_0^{2}}{\rho a}, B_0=\frac{B}{x^{\frac{n-1}{2}}}, \Lambda_1=\lambda_1 a x^{n-1}, \Lambda_2=\frac{\lambda_2 a x^{n-1}}{\upsilon}, \mathrm{Re}_x=\frac{xu_w}{\upsilon},\\ R=\frac{16}{3}\frac{\sigma^* T_\infty^{3}}{kk^*}, \Pr=\frac{\mu C_p}{k}, Ec=\frac{u_w{}^{2}}{C_p\left(T_w-T_\infty\right)}, \lambda=\frac{Gr}{\mathrm{Re}_x^{2}}, Gr=\frac{g\beta_T\left(T_w-T_\infty\right)x^{3}}{\upsilon^{2}}.\end{array}\right\}$$

The friction factor can be expressed as follows:

$$Cf=\left.\frac{\tau_w}{\frac{1}{2}\rho u_w{}^{2}}\right|_{y=0}, \tau_w=\mu\left(\frac{\partial u}{\partial y}\right). \tag{9}$$

The use of (5) facilitates a more straightforward formulation of the equation presented in (9) as follows:

$$\sqrt{\mathrm{Re}_x}Cf=\sqrt{2\left(n+1\right)}f''(0).$$

The subsequent formula can be used to determine the Nusselt number:

$$Nu=\frac{-x}{k_f\left(T_w-T_\infty\right)}\left(k+\frac{16\sigma^* T_\infty^{3}}{k^*}\right)\left.\frac{\partial T}{\partial y}\right|_{y=0}. \tag{10}$$

By employing (5), the formula utilized in (10) can be succinctly reformulated as:

$$\left(\mathrm{Re}_x\right)^{-1/2}Nu=-\sqrt{\frac{n+1}{2}}\left(1+R\right)\theta'(0).$$

The formula that describes the dimensional computation of entropy production is mentioned as:

$$S_g=\left(\frac{k_f}{T_\infty^{2}}\right)\left(1+16\frac{\sigma^* T_\infty^{3}}{3kk^*}\right)\left(\frac{\partial T}{\partial y}\right)^{2}+\frac{\mu}{T_\infty}\left(\frac{\partial u}{\partial y}\right)^{2}+\frac{\sigma}{T_\infty}u^{2}B^{2}. \tag{11}$$

By adopting (5), we may rewrite equation (11) as follows:

$$N_{EG}=\frac{n+1}{2}\left(1+R\right)\alpha_1\theta'^{2}+\frac{n+1}{2}Brf''^{2}+MBrf'^{2},$$

Where

$$N_{EG}=\frac{\upsilon T_\infty x S_g}{ku_w\left(T_w-T_\infty\right)}, Br=\frac{\mu u_w{}^{2}}{k\left(T_w-T_\infty\right)}.$$

Numerical Procedure

The boundary value problem represented by equations (6) and (7), subject to the constraints in (8), is solved numerically using the bvp4c solver in MATLAB. This computational tool implements a collocation method based on the three-stage Lobatto IIIa

formula, which efficiently transforms the original differential equations into an algebraic system. By providing an initial guess for the solution profile, the algorithm iteratively refines the approximation until it converges to a continuous solution that satisfies all specified boundary conditions with high accuracy. This approach is particularly effective for handling the multipoint and potentially nonlinear nature of the problem defined by the given equations.

Results and discussion

As seen in Fig. 2, increasing the magnetic field strength reduces the flow velocity. This occurs because the applied magnetic field induces a resistive Lorentz force, which opposes the fluid motion. Fig. 3 indicates that an increase in the couple stress parameter corresponds to a reduction in the fluid's velocity profile. This occurs because the couple stress parameter represents the influence of internal rotational resistance within the fluid microstructure. A higher value of this parameter enhances the effective viscosity or internal friction, thereby imposing a greater resistive force against fluid motion. Consequently, the flow experiences more damping, which manifests as a noticeable decrease in velocity across the channel. Fig. 4 indicates that increasing the retardation parameter within the Oldroyd fluid model results in a reduced fluid velocity. This occurs because the retardation parameter governs the timescale over which the fluid relaxes from its elastic, solid-like response to its viscous, liquid-like behavior. A higher value signifies a longer retardation time, meaning the fluid resists deformation for a greater duration. Consequently, this enhanced internal resistance to flow, stemming from its persistent elastic character, acts as a damping mechanism, ultimately suppressing the overall velocity profile. Fig. 5 indicates that an increase in the Prandtl number corresponds to a reduction in the fluid temperature. This occurs because a higher Prandtl number signifies a fluid with a lower thermal diffusivity relative to its momentum diffusivity. Consequently, the transfer of heat by conduction becomes less effective compared to the transport of momentum. This weakened thermal diffusion restricts the propagation of heat from the heated surface into the fluid bulk, resulting in a steeper temperature gradient near the boundary and an overall lower temperature within the fluid domain. Fig. 6 indicates that an increase in the Eckert number corresponds to a higher temperature within the fluid. This behavior can be attributed to the physical interpretation of the Eckert number, which represents the ratio of kinetic energy to enthalpy difference. A larger Eckert number signifies that the energy dissipated due to viscous friction, or the conversion of kinetic energy into internal energy, becomes more significant. Consequently, this enhanced viscous dissipation acts as an internal heat source, resulting in greater thermal energy within the fluid and thus elevating its overall temperature. Fig. 7 indicates that an increase in the thermal radiation parameter corresponds to a higher temperature within the fluid. This occurs because enhanced thermal radiation contributes additional energy to the system, effectively serving as an extra heat source. Consequently, the fluid absorbs more thermal energy, leading to a measurable elevation in its overall temperature profile. Fig. 8 indicates that increasing the Brinkman number results in greater entropy generation within the fluid flow. This relationship occurs because the Brinkman number represents the relative importance of viscous heat dissipation compared to conductive heat transfer. A higher value signifies more significant frictional heating due to viscosity. This enhanced viscous dissipation acts as an irreversible source of internal thermal energy, thereby directly increasing the disorder and irreversibility in the system, which is quantified as a rise in entropy generation. Fig. 9 indicates that increasing the thermal radiation parameter enhances the rate of entropy generation within the fluid flow. This occurs because greater radiative heat transfer introduces additional thermal gradients and energy dissipation into the system. Consequently, the overall irreversibility associated with heat transfer and fluid friction is amplified, leading to a higher total entropy production. This relationship highlights the significant role of radiation in augmenting thermodynamic losses in the flow.

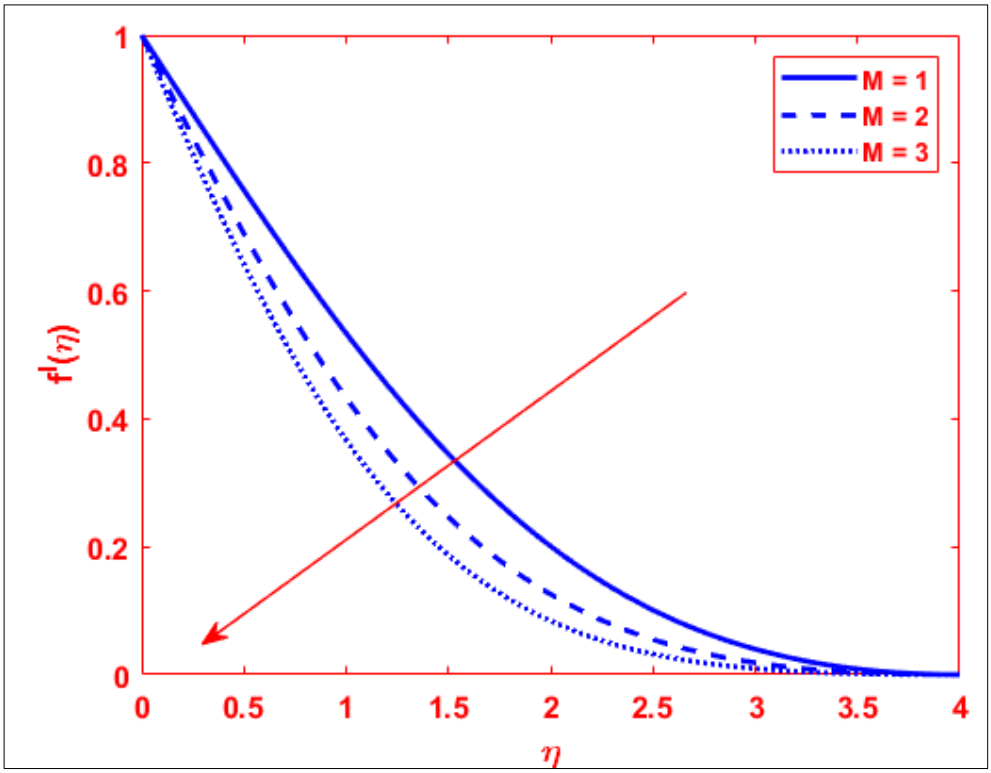

Fig 2: Influence of M on velocity profile

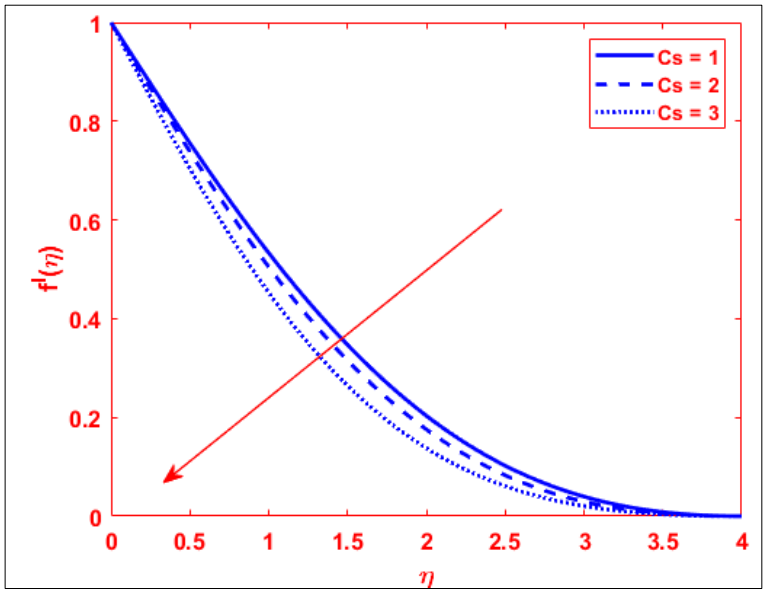

Fig 3: Influence of Cs on velocity profile

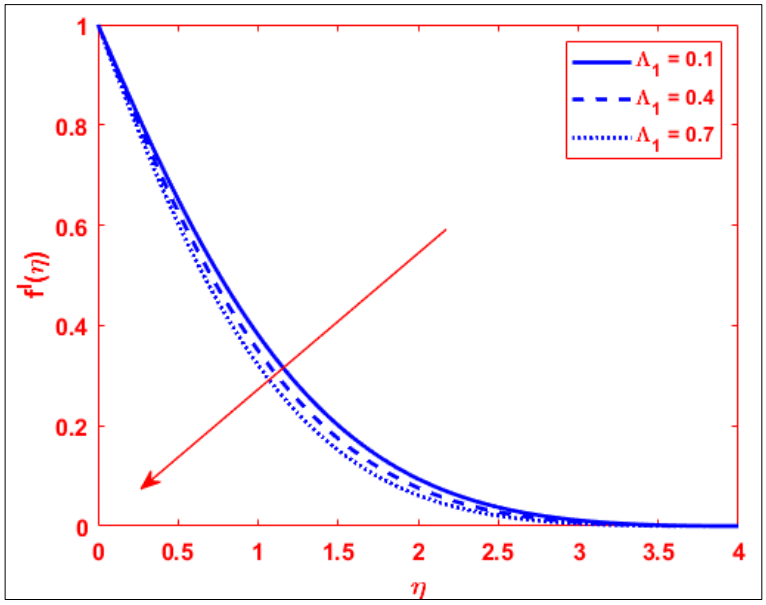

Fig 4: Influence of Λ_1 on velocity profile

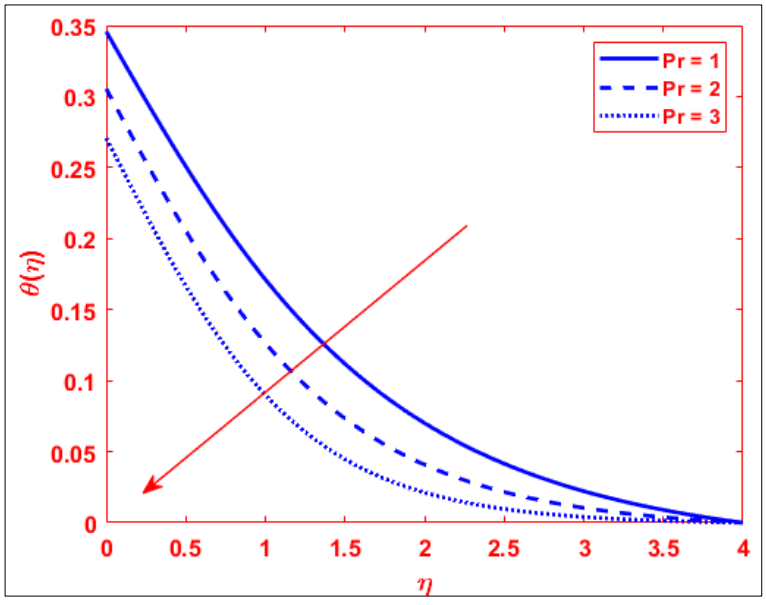

Fig 5: Influence of Pr on velocity profile

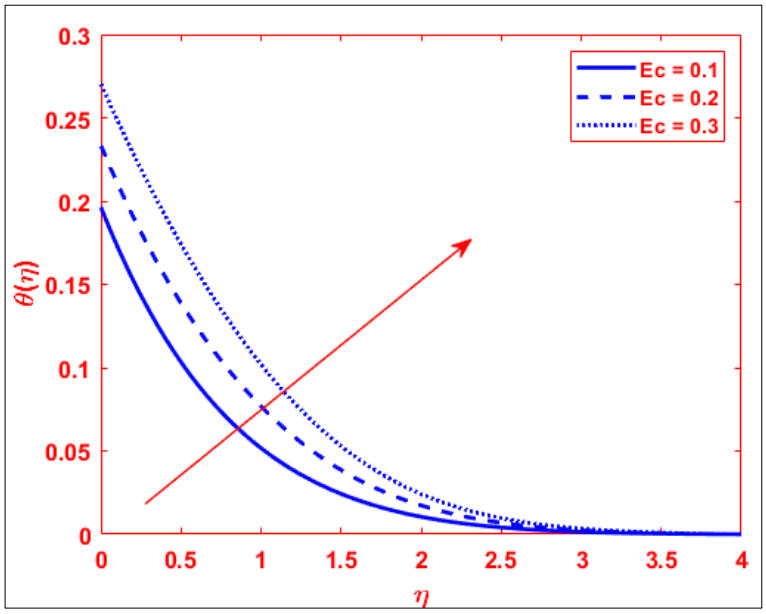

Fig 6: Influence of Ec on temperature profile

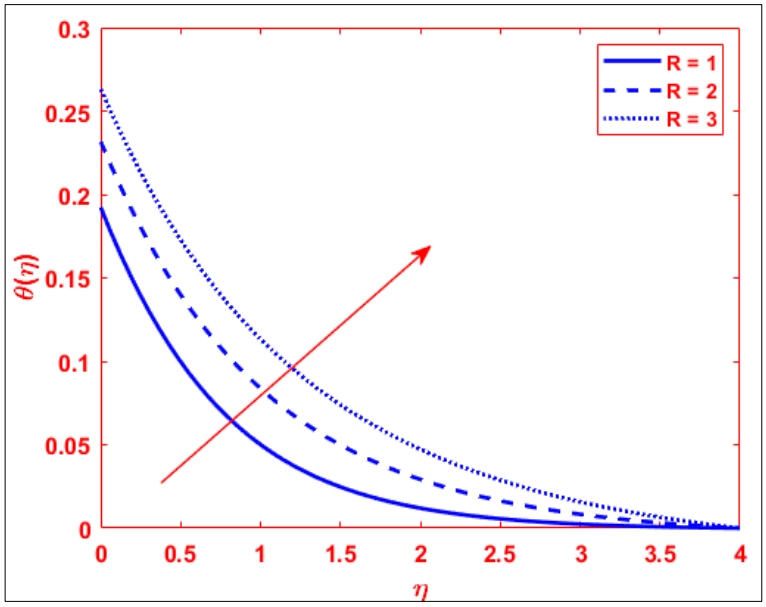

Fig 7: Influence of R on temperature profile

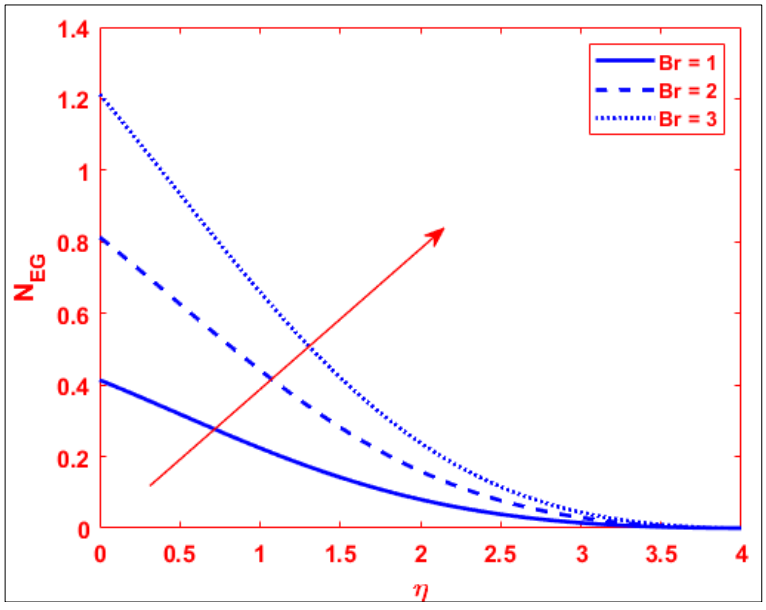

Fig 8: Influence of Br on entropy generation profile

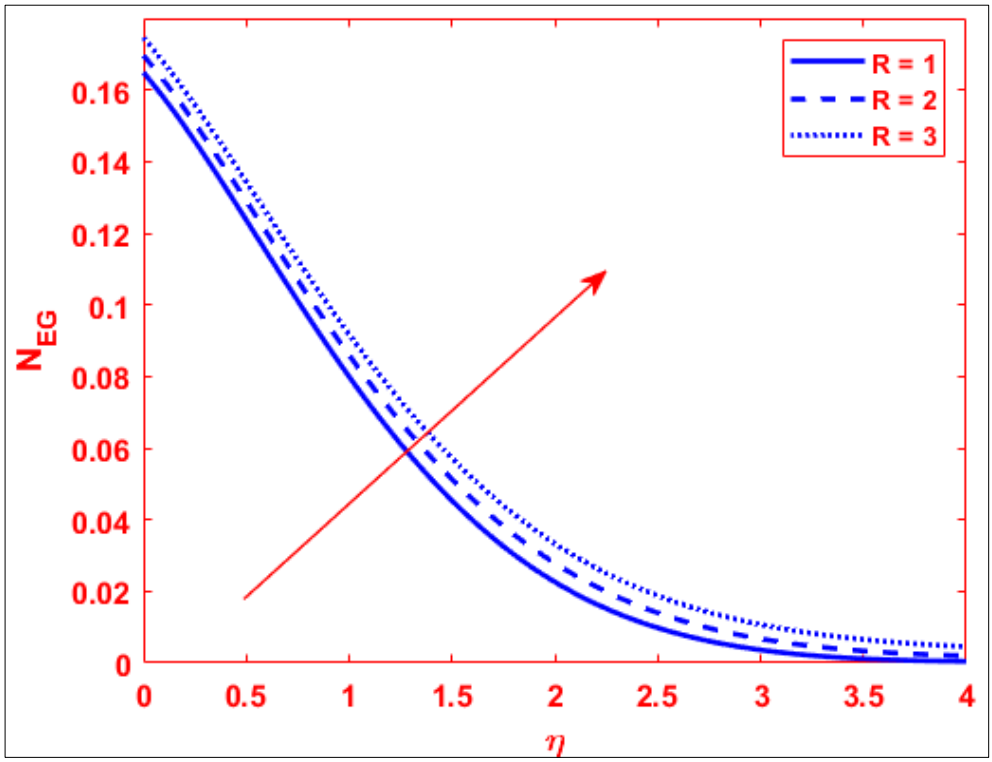

Fig 9: Influence of R on entropy generation profile

Multiple Linear Regression

Multiple linear regression is a statistical method used to model the relationship between a single dependent variable and two or more independent variables. By fitting a linear equation to observed data, this technique estimates how each predictor variable contributes to changes in the outcome while holding the others constant. It allows researchers to assess the collective influence of several factors simultaneously, providing insights into their relative importance and predictive power. The method is widely applied across disciplines such as economics, social sciences, and engineering to analyze complex, multi-faceted relationships.

In this study, MLR was used to correlate the influential physical parameters directly with the key engineering quantities of interest: the skin friction coefficient and the Nusselt number. The general forms of the proposed models are:

$$Cf = a_0 + a_1 M + a_2 Cs + a_3 \lambda \quad (12)$$

$$Nu = b_0 + b_1 R + b_2 Pr + b_3 Ec \quad (13)$$

Utilizing 25 distinct numerical data sets for each correlation, the following specific regression equations were derived:

$$Cf = = 0.6862 + 0.0181M + +0.0809Cs - 0.0062\lambda \quad (14)$$

$$Nu = 0.1844 + 0.1373R + 0.0149Pr - 0.0604Ec \quad (15)$$

Equation 14, derived through multiple linear regression, models the skin friction coefficient (Cf) as a function of three key parameters. The positive coefficients for the magnetic field (M) and the couple stress parameter (Cs) indicate that an increase in either factor contributes to a higher skin friction coefficient. Conversely, the negative coefficient for the mixed convection parameter (λ) shows that its influence acts to reduce the skin friction. The constant term of 0.6862 represents the baseline value of Cf when all three explanatory variables are zero. An increase in the mixed convection parameter reflects a stronger influence of buoyancy forces relative to forced convection. Enhanced buoyancy typically accelerates the fluid near the boundary, reducing the velocity gradient between the surface and the free stream. Since skin friction coefficient is directly proportional to this velocity gradient at the wall, a reduction in the gradient results in a lower frictional resistance. Consequently, the intensified mixed convection effect acts to diminish the shear stress at the surface, leading to a decrement in Cf as mathematically indicated by its negative coefficient in the regression model. Based on the results of a multiple linear regression analysis, Equation 15 models the Nusselt number (Nu) as a function of three key dimensionless parameters. The positive coefficients for the thermal radiation parameter (R) and the Prandtl number (Pr) indicate that an increase in either of these variables enhances the rate of convective heat transfer, as reflected by a higher Nu value. Conversely, the negative coefficient for the Eckert number (Ec) suggests that greater viscous dissipation acts to reduce the overall heat transfer performance. The negative influence of the Eckert number on the Nusselt number can be attributed to the role of viscous dissipation. A higher Ec signifies that a greater portion of the fluid's kinetic energy is converted into thermal energy due to internal friction. This self-generated heat acts as an internal heat source within the boundary layer. Consequently, it elevates the fluid temperature near the surface, which reduces the temperature gradient between the surface and the mainstream flow. Since the Nusselt number is directly proportional to this temperature gradient, its value diminishes as the gradient weakens.

Validation of the results using Bayesian neural network approach

To ensure the robustness of the findings, a Bayesian neural network (BNN) was employed for validation. Unlike conventional neural networks that yield single-point estimates, a BNN treats the model's weights as probability distributions rather than fixed values. This framework naturally quantifies predictive uncertainty by generating a distribution of possible outputs for each input. Consequently, the validation process assesses not just the model's accuracy, but also the reliability of its predictions. Predictions with high uncertainty can be flagged for further scrutiny, while the model's overall confidence can be evaluated across the dataset. This approach provides a statistically grounded measure of trust in the results, moving beyond mere point estimates to a more comprehensive probabilistic evaluation of model performance.

Figure 10 demonstrates that the Bayesian neural network learns the dependence of the skin friction-related output on the mixed convection parameter with extremely high numerical accuracy, as the mean squared error (MSE) collapses by roughly nine orders of magnitude within only ten epochs. At the start of training (epoch 0), the MSE for both the training and testing sets is close to 10^{-2}, but by epoch 2 it has already fallen to the order of 10^{-5} - 10^{-6}, and then continues to decay steadily through intermediate levels around 10^{-7}, 10^{-8}, and 10^{-9} as the epochs progress. Near epochs 8-9, the curves lie in the 10^{-10} range, and the best recorded training performance reaches approximately 1.09×10^{-11} at epoch 10, indicating an almost negligible average squared discrepancy between the network predictions of skin friction and the reference data over the explored mixed-convection regime. The function-fit plot in Fig. 11 confirms that the Bayesian neural network almost perfectly reconstructs the relationship between the mixed convection parameter and the corresponding skin-friction-related output over the entire input domain. In the upper panel, the continuous fitted line coincides with the densely packed training and testing markers, which collectively trace a nearly straight, monotonically decreasing profile from roughly −0.35 at the lowest input value to about −0.54 at the highest, indicating an approximately linear reduction of the skin friction coefficient with increasing mixed convection parameter in this range. The lower error panel shows that the pointwise differences between targets and predictions remain confined to a very narrow band on the order of 10^{-5}, with small, oscillatory fluctuations around zero and only a few slightly larger spikes near the upper end of the input interval, demonstrating that the model captures virtually all of the variance in the data with negligible systematic bias or drift.

The performance curve (Fig. 12) associated with the Bayesian neural network indicates that the model learns the influence of the thermal radiation parameter on the Nusselt number with exceptional accuracy, as the mean squared error (MSE) drops by many orders of magnitude over 1000 training epochs. Initially the MSE for both training and testing data is of order 10^{0}, but it falls sharply within the first few epochs and then continues to decrease gradually to the 10^{-11} - 10^{-12} range, where the best training performance reaches about 2.35×10^{-12} at epoch 1000, while the blue (training) and red (test) curves remain closely aligned throughout, confirming very strong generalization without noticeable overfitting. Fig. 13 shows that the Bayesian neural network reproduces the dependence of the Nusselt number on the thermal radiation parameter with almost perfect linearity and extremely small prediction errors. In the upper panel, the fitted curve forms an almost straight, increasing line from about 0.25 to roughly 3.0 as the input rises from 0 to 20, while the training and testing markers lie directly on this line, indicating that the network accurately captures the strengthening of convective heat transfer with increasing radiation effects. The lower error panel reveals that the differences between target and predicted Nusselt numbers are confined to a narrow band of order 10^{-6}, with only small oscillations around zero, confirming that the Bayesian model provides a highly precise and unbiased mapping between thermal radiation intensity and the Nusselt number.

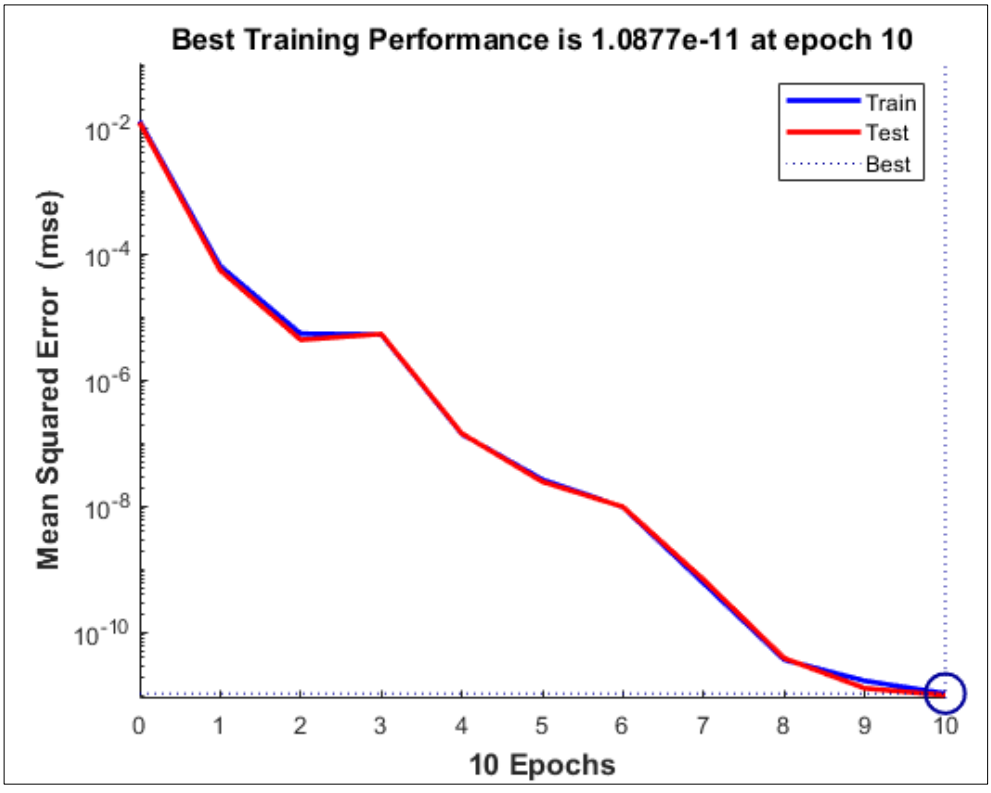

Fig 10: Mean squared error (MSE) vs training epoch for mixed convection parameter vs skin friction coefficient

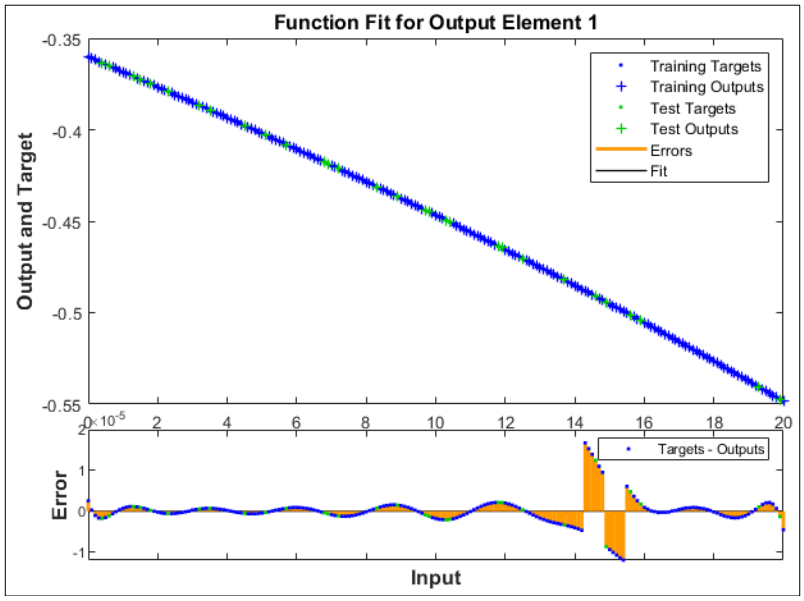

Fig 11: Function fit plot for mixed convection parameter vs skin friction coefficient

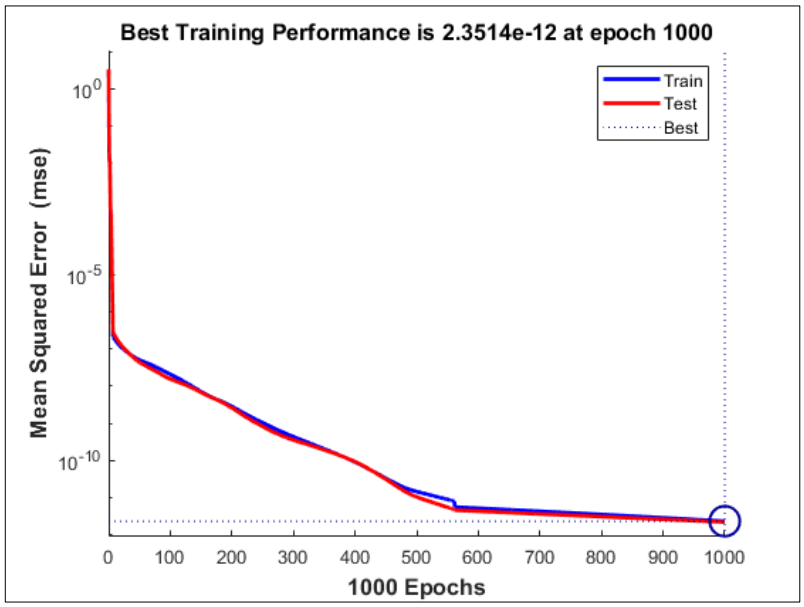

Fig 12: Mean squared error (MSE) vs training epoch for thermal radiation parameter vs Nusselt number

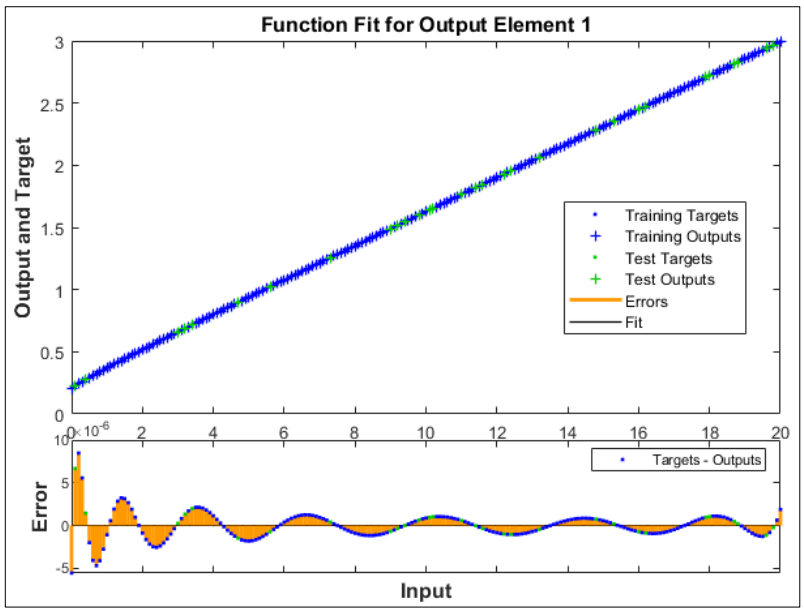

Fig 13: Function fit plot for thermal radiation parameter vs Nusselt number

Conclusion

This study has conducted a numerical investigation into the steady magnetohydrodynamic flow, heat transfer, and entropy generation of a couple stress Oldroyd-B fluid over a wedge. The governing system, incorporating thermal radiation and Joule heating effects, was transformed into ordinary differential equations via similarity variables and subsequently solved using the high-accuracy bvp4c collocation method in MATLAB. The primary physical insights and predictive outcomes are summarized as follows:

- The fluid velocity profile is significantly inhibited by an increase in both the magnetic field parameter and the couple stress parameter. The magnetic field generates a resistive Lorentz force, while the couple stress enhances internal rotational resistance, both acting to dampen the flow.
- The fluid temperature is elevated by increases in the Eckert number (Ec) and the thermal radiation parameter. A higher Ec amplifies viscous dissipation as an internal heat source, and a larger R contributes additional radiative energy to the system.
- An increase in the Prandtl number (Pr) reduces the temperature profile, as a higher Pr indicates lower thermal diffusivity, restricting conductive heat penetration from the surface.
- Entropy generation within the flow is augmented by raising the Brinkman number (Br) and the thermal radiation parameter. A higher Br signifies greater irreversible viscous heating, while enhanced radiation introduces steeper thermal gradients.
- From the numerical data, explicit multiple linear regression correlations were successfully developed for the skin friction coefficient (Cf) and the Nusselt number (Nu). The model for Cf shows a positive dependence on M and Cs, but a negative dependence on the mixed convection parameter (λ). The model for Nu increases with R and Pr, but decreases with Ec.
- The predictive accuracy and generalization capability of the derived regression models were rigorously validated using a Bayesian neural network (BNN) approach. The BNN achieved an exceptionally low mean squared error, confirming the high fidelity of the numerical data and the statistical reliability of the empirical correlations.

References

1. Dawar A, Shah Z, Tassaddiq A, Kumam P, Islam S, Khan W. A convective flow of Williamson nanofluid through cone and wedge with non-isothermal and non-isosolutal conditions: a revised Buongiorno model. Case Stud Therm Eng. 2021;24:100869.
2. Shahzad U, Mushtaq M, Farid S, Jabeen K, Muntazir RMA. A numerical approach for an unsteady tangent hyperbolic nanofluid flow past a wedge in the presence of suction/injection. Math Probl Eng. 2021;2021(1):8653091.
3. Kudenatti RB, Misbah NE, Bharathi MC. Stability of hydromagnetic boundary layer flow of non-Newtonian power-law fluid flow over a moving wedge. Eng Comput. 2022;38(2):1107-1126.
4. Dharmaiah G, Sridhar W, Al-Farhany K, Balamurugan KS, Ali F. Non-Newtonian nanofluid characteristics over a melting wedge: a numerical study. Heat Transfer. 2022;51(5):4620-4640.
5. Zulqarnain RM, Nadeem M, Siddique I, Ahmad H, Askar S, Samar M. Heat transfer analysis of Maxwell tri-hybridized nanofluid through Riga wedge with fuzzy volume fraction. Sci Rep. 2023;13(1):18238.
6. Ali B, Ilyas M, Siddique I, Yang H, Ashraf MK, Abdal S. Numerical study for bio-convection effects on MHD nanofluid flow past a porous and extending wedge. Propuls Power Res. 2023;12(4):584-594.
7. Azar AA, Jalili P, Moziraji ZP, Jalili B, Ganji DD. Analytical solution for MHD nanofluid flow over a porous wedge with melting heat transfer. Heliyon. 2024;10(15):eXXXXX.
8. Rajput S, Verma AK, Bhattacharyya K, Chamkha AJ. Unsteady nonlinear mixed convective flow of nanofluid over a wedge: Buongiorno model. Waves Random Complex Media. 2024;34(5):4059-4073.
9. Kumar H, Rawat SK, Yaseen M, Pant M, Singh SJ. Analysis of the heat transfer in a Maxwell-based non-Newtonian ternary hybrid nanofluid flow over a wedge surface with an advanced soft computing method. Pramana. 2025;99(4):175.
10. Bharathi V, Prakash J. Zeta potential and activation energy effects in an EMHD non-Newtonian nanofluid flow over a wedge with Darcy-Forchheimer porous medium. Numer Heat Transf A Appl. 2025;86(16):5557-5584.
11. Acharya N, Mondal H, Kundu PK. Spectral approach to study the entropy generation of radiative mixed convective couple stress fluid flow over a permeable stretching cylinder. Proc Inst Mech Eng C J Mech Eng Sci. 2021;235(15):2692-2704.
12. Ullah H, Hayat T, Ahmad S, Alhodaly MS. Entropy generation and heat transfer analysis in power-law fluid flow: finite difference method. Int Commun Heat Mass Transf. 2021;122:105111.
13. Berrehal H, Dinarvand S, Khan I. Mass-based hybrid nanofluid model for entropy generation analysis of flow upon a convectively-warmed moving wedge. Chin J Phys. 2022;77:2603-2616.
14. Reedy S, Srihari P, Ali F, Naikoti K. Numerical analysis of Carreau fluid flow over a vertical porous microchannel with entropy generation. Partial Differ Equ Appl Math. 2022;5:100304.
15. Ali A, Ahmed M, Ahmad A, Nawaz R. Enhanced heat transfer analysis of hybrid nanofluid over a Riga plate: incorporating Lorentz forces and entropy generation. Tribol Int. 2023;188:108844.
16. Iftikhar B, Javed T, Siddiqu MA. Entropy generation analysis during MHD mixed convection flow of non-Newtonian fluid saturated inside the square cavity. J Comput Sci. 2023;66:101907.
17. Kumar S, Sharma K, Makinde OD, Joshi VK, Saleem S. Entropy generation in water conveying nanoparticles flow over a vertically moving rotating surface: Keller box analysis. Int J Numer Methods Heat Fluid Flow. 2024;34(2):608-628.
18. Olkha A, Kumar M, Choudhary R. Entropy generation in third-grade non-Newtonian fluid flow and heat transport through porous medium in a horizontal channel under heat generation. Trends Sci. 2024;21(11):6966.
19. Jat K, Sharma K, Choudhary P, Soni P. Entropy generation analysis of couple stress Casson fluid flow through non-permeable stretching channel. Eur Phys J Spec Top. 2025;234:1-20.
20. Majeed AH, Mahmood R, Liu D, Ullah S. Numerical simulations of entropy generation and thermal fluid flow in a wavy enclosure: a Newton-Pardiso solver-based study. Int Commun Heat Mass Transf. 2025;162:108569.
21. Bilal AM, Hayat T, Alsulami H. Mixed convection Falkner-Skan wedge flow of an Oldroyd-B fluid in presence of thermal radiation. 2016.